Supporting Information for Factors Governing Oxygen Vacancy Formation in Oxide Perovskites

Robert B. Wexler†, Gopalakrishnan Sai Gautam†, Ellen B. Stechel§, and Emily A. Carter†,‡

†Department of Mechanical and Aerospace Engineering, Princeton University, Princeton, NJ 08544-5263, United States, § ASU Lightworks and the School of Molecular Sciences, Arizona State University, Tempe, Arizona 85287-5402, United States, and ‡ Office of the Chancellor and Department of Chemical and Biomolecular Engineering, University of California, Los Angeles, Los Angeles, CA 90095, United States

Table S1. Computational cost associated with PBE, PBE+*U*=3.9,[1] SCAN, and SCAN+*U*=2.7[2] self-consistent-field calculations for four "high quality" experimental crystal structures of $BaMnO_3$. ICSD is the Inorganic Crystal Structure Database Collection Code and *t* is time. Input parameters are the same as those in the main text.

ICSD	Space Group		# Atoms	XC	*U*	*t* (s)	# Steps	t_s=*t*/step	min(*t*)	*t*/min(*t*)	min(t_s)	t_s/min(t_s)
10250	$P6_3/mmc$	194	40	PBE	0.0	1077	21	51	939	1.15	51	1.00
10250	$P6_3/mmc$	194	40	PBE	3.9	939	18	52	939	1.00	51	1.02
10250	$P6_3/mmc$	194	40	SCAN	0.0	2402	22	109	939	2.56	51	2.13
10250	$P6_3/mmc$	194	40	SCAN	2.7	1997	21	95	939	2.13	51	1.85
66822	$R\bar{3}m$	166	54	PBE	0.0	1290	19	68	1287	1.00	68	1.00
66822	$R\bar{3}m$	166	54	PBE	3.9	1287	19	68	1287	1.00	68	1.00
66822	$R\bar{3}m$	166	54	SCAN	0.0	2770	22	126	1287	2.15	68	1.86
66822	$R\bar{3}m$	166	54	SCAN	2.7	3024	21	144	1287	2.35	68	2.13
89994	$P6_3/mmc$	194	10	PBE	0.0	192	19	10	166	1.16	10	1.00
89994	$P6_3/mmc$	194	10	PBE	3.9	166	16	10	166	1.00	10	1.03
89994	$P6_3/mmc$	194	10	SCAN	0.0	411	20	21	166	2.48	10	2.03
89994	$P6_3/mmc$	194	10	SCAN	2.7	333	15	22	166	2.01	10	2.20
89995	$P6_3cm$	185	30	PBE	0.0	1189	22	54	764	1.56	45	1.20
89995	$P6_3cm$	185	30	PBE	3.9	764	17	45	764	1.00	45	1.00
89995	$P6_3cm$	185	30	SCAN	0.0	1612	18	90	764	2.11	45	1.99
89995	$P6_3cm$	185	30	SCAN	2.7	1435	16	90	764	1.88	45	2.00

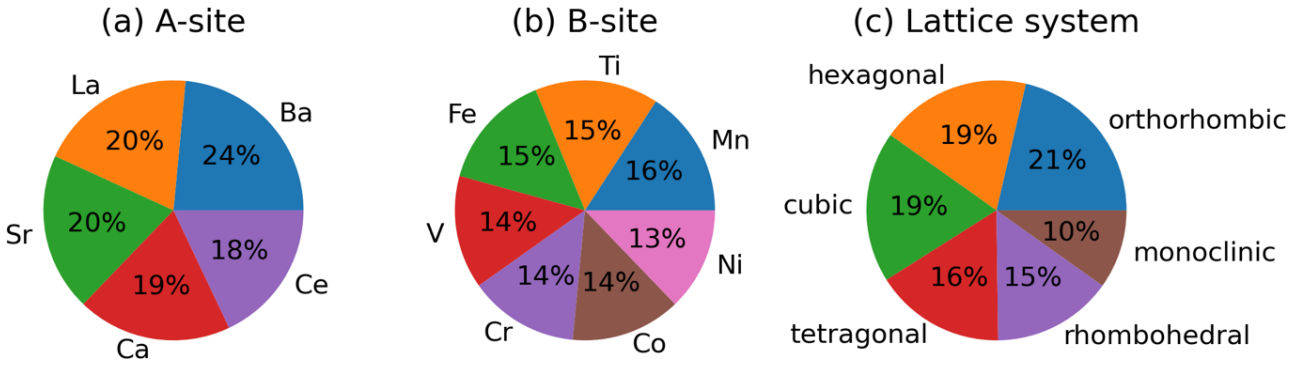

Figure S1. Distribution of ABO_3 perovskite structures in the bulk by (a) A-site, (b) B-site, and (c) lattice system. We tabulated structures, total free energies, energies for $\sigma \rightarrow 0$ where σ is the width of the Gaussian smearing, magnetizations, local charges and magnetic moments, and band gaps for pristine primitive cells and supercells in bulk.csv.

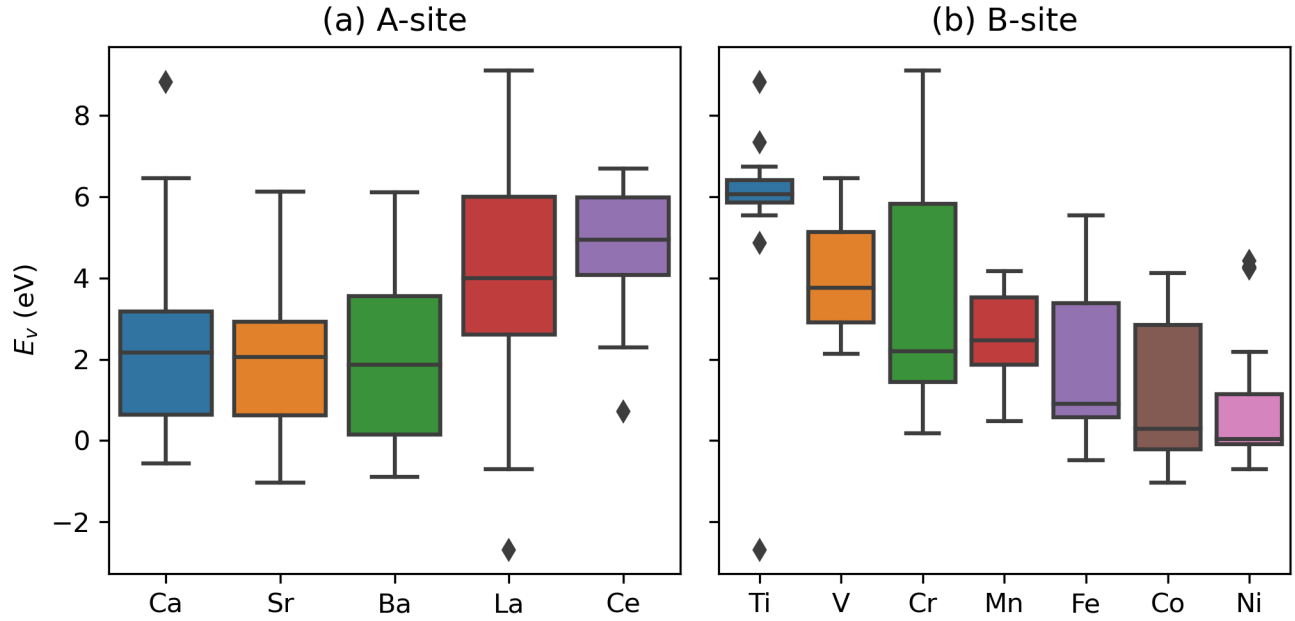

Figure S2. Distribution of neutral oxygen vacancy formation energies (E_v) for ABO_3 perovskite structures by (a) A-site and (b) B-site. The boxes show the quartiles of the data subsets while the whiskers show the rest of the distribution, except for points that are outside 1.5×IQR (diamonds) where IQR is the interquartile range. We tabulated structures, total free energies, energies for $\sigma \rightarrow 0$, magnetizations, local charges and magnetic moments, band gaps, and E_v for defective supercells in defects.csv.

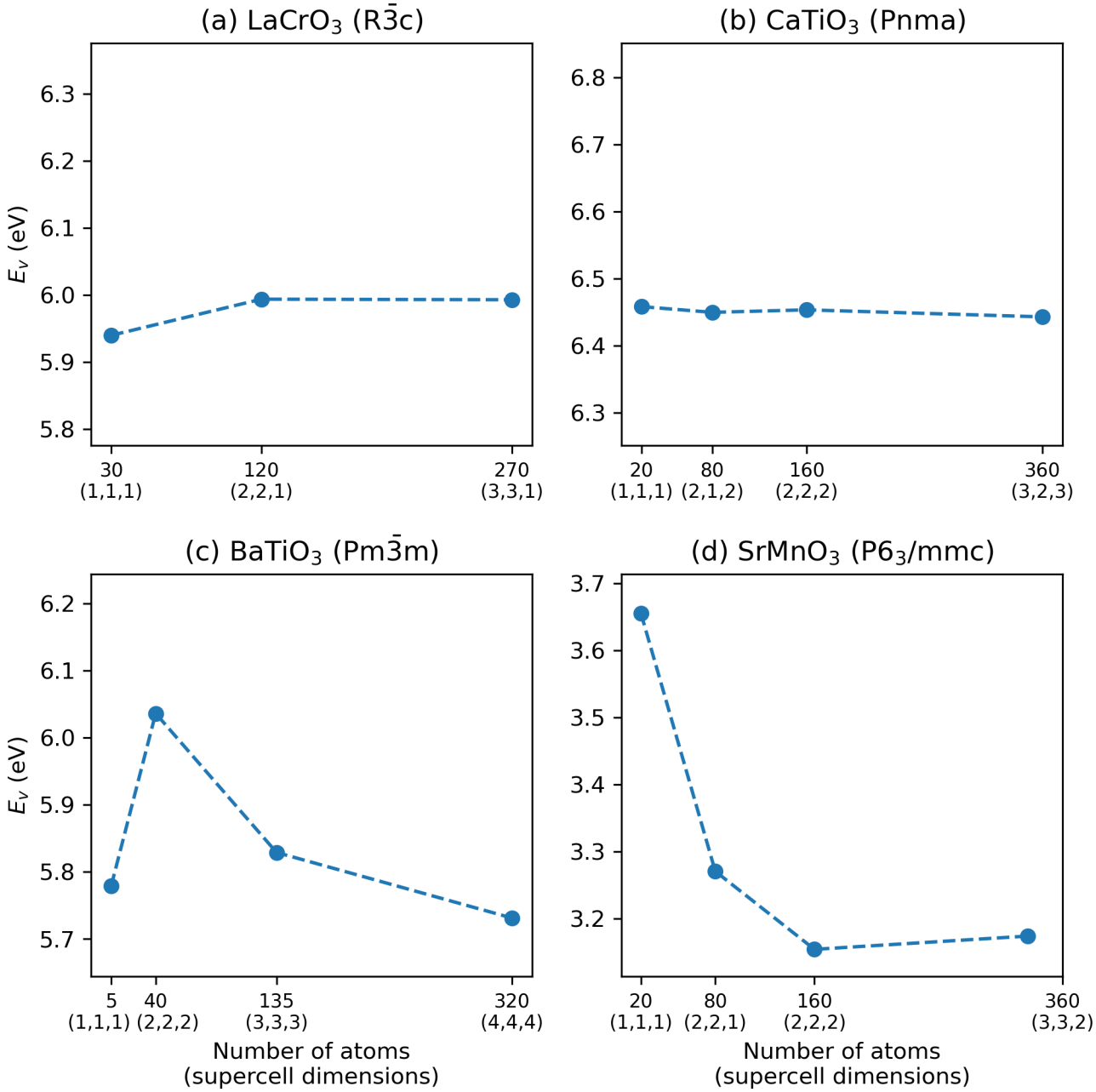

Figure S3. Convergence of E_v in (a) $LaCrO_3$ ($R\bar{3}c$), (b) $CaTiO_3$ ($Pnma$), (c) $BaTiO_3$ ($Pm\bar{3}m$), and (d) $SrMnO_3$ ($P6_3/mmc$). We did not explicitly perform convergence tests for tetragonal ($P4mm$) and monoclinic ($P2_1/b$) structures since they share similar lattice parameters with cubic ($Pm\bar{3}m$) and orthorhombic ($Pnma$) structures, respectively.

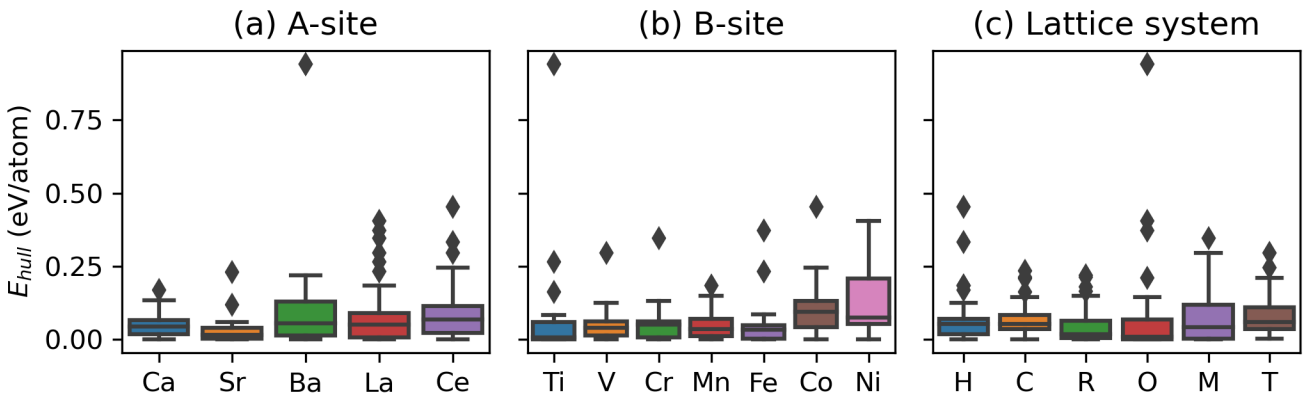

Figure S4. Distribution of energies above the convex hull (E_{hull}) for ABO_3 perovskite structures by (a) A-site, (b) B-site, and (c) lattice system. The boxes show the quartiles of the data subsets while the whiskers show the rest of the distribution, except for points that are outside 1.5×IQR (diamonds) where IQR is the interquartile range.

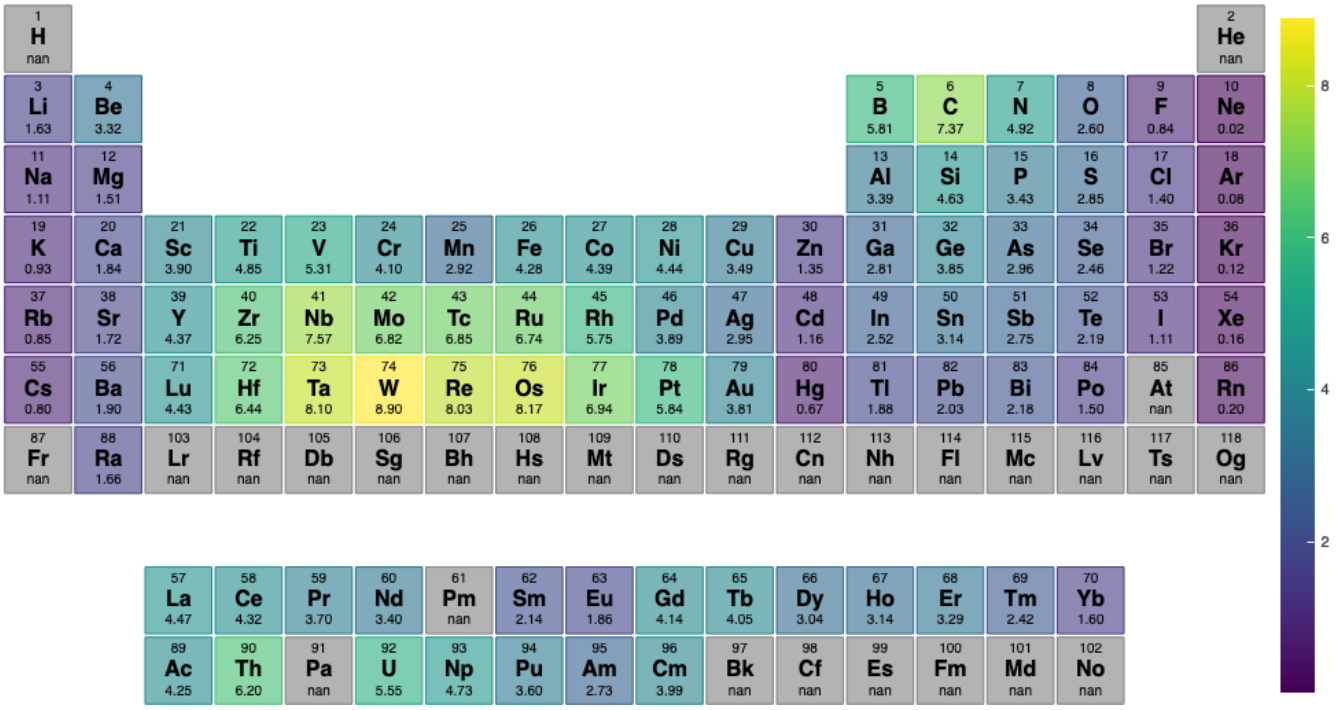

Figure S5. Periodic trends in experimental cohesive energies in eV/atom,[3] listed below each element. We tabulated cohesive energies in element_cohesive_energies.csv. "nan" indicates unavailability of experimental cohesive energies (grey squares).

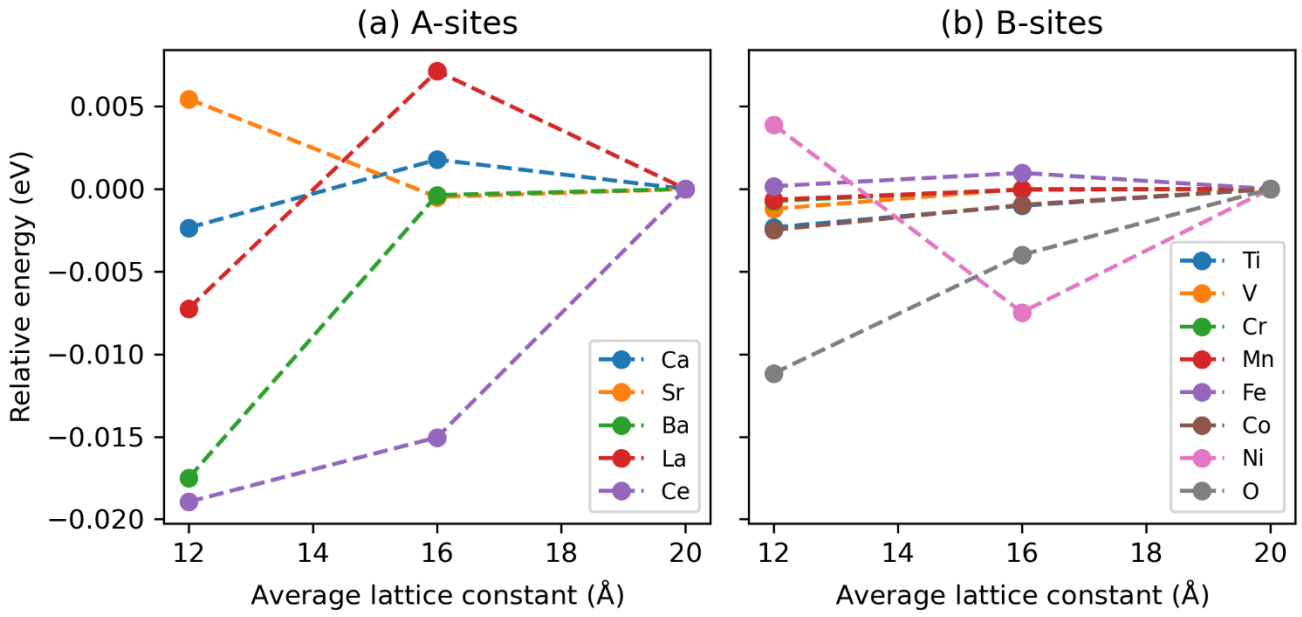

Figure S6. Cell-size convergence of total energies for neutral (a) A- and (b) B-site atoms in their electronic ground states. We tabulated atomic total energies in atoms.csv.

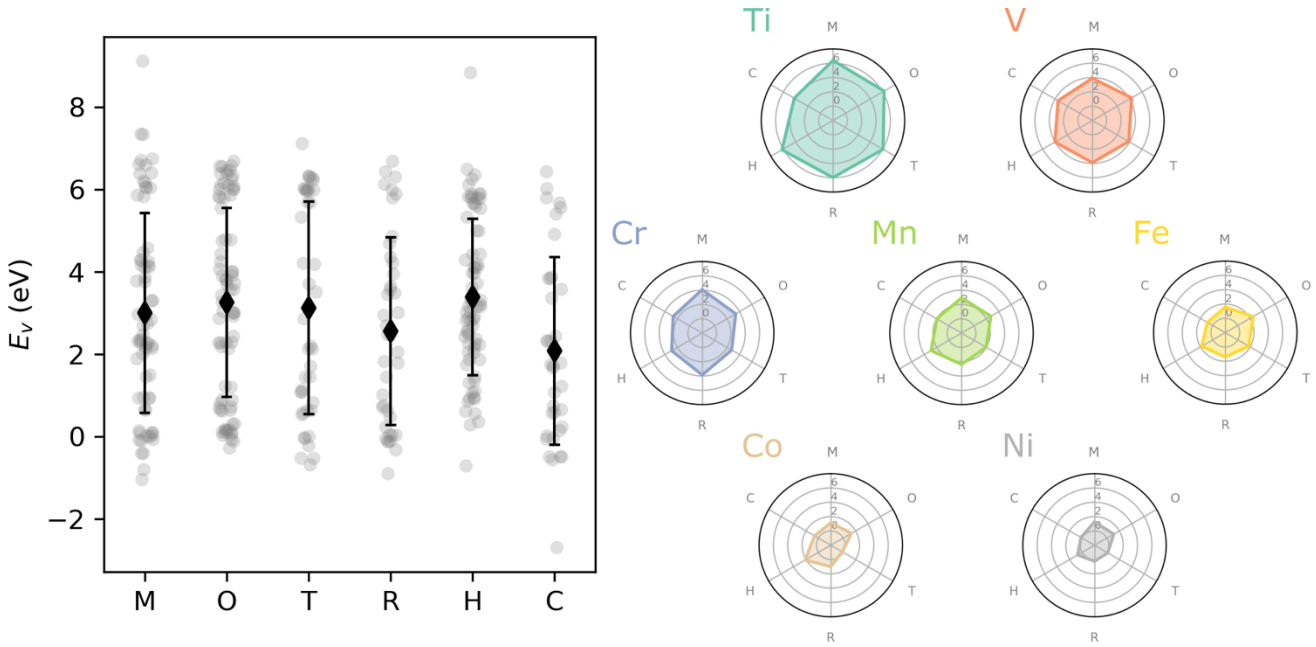

Figure S7. Effect of crystal system on E_v where M, O, T, R, H, and C are monoclinic, orthorhombic, tetragonal, rhombohedral, hexagonal, and cubic, respectively. Error bars show the standard deviation of E_v. All data are shown on the left whereas the data are collated by B-cation on the right (averages are shown as vertices along each crystal system axis). The left panel shows that no direct correlation exists between crystal system and E_v. On the other hand, **Figure 6** in the main text shows a strong correlation between E_b, V_r, and E_v. Since **Equations 2** and **5** in the main text indicate that E_b and V_r are structure independent while **Equation 9** in the main text reveals that V_r typically is that of the B-site cation, we

also sorted by B-site cation (right panel) to uncover any further correlations. Still, only a weak, direct correlation is evident between crystal system and E_v in the right panel (given by the degree of distortion away from a regular hexagon). Given that the two other descriptors in our model, E_g and E_{hull}, are indeed structure dependent, it appears that a weak, indirect correlation exists between crystal system and E_v via E_g and E_{hull}.

Table S2. Theoretical and experimental cohesive energies (E_c) across all metal oxides considered.

Metal oxide	SCAN+*U* E_c (eV)	Exp[3–6] E_c (eV)	Relative error (eV)
CaO	11.30	11.00	0.30
SrO	10.54	10.44	0.11
BaO	10.20	10.22	-0.02
La_2O_3	34.94	35.28	-0.33
Ce_2O_3	34.74	35.27	-0.53
CeO_2	20.51	20.78	-0.27
TiO_2	18.96	19.81	-0.84
VO_2	17.41	17.87	-0.46
CrO_2	15.68	15.30	0.38
MnO_2	13.52	13.48	0.05
FeO_2	12.75	n/a	n/a
CoO_2	12.07	n/a	n/a
NiO_2	11.76	n/a	n/a
Ti_2O_3	31.46	33.21	-1.75
V_2O_3	30.34	31.00	-0.66
Cr_2O_3	27.88	27.66	0.22
Mn_2O_3	23.62	23.51	0.11
Fe_2O_3	24.80	24.82	-0.02
Co_3O_4	33.12	32.88	0.23
Ni_2O_3	21.68	21.70	-0.02
CoO	9.56	9.45	0.11
NiO	9.57	9.52	0.05

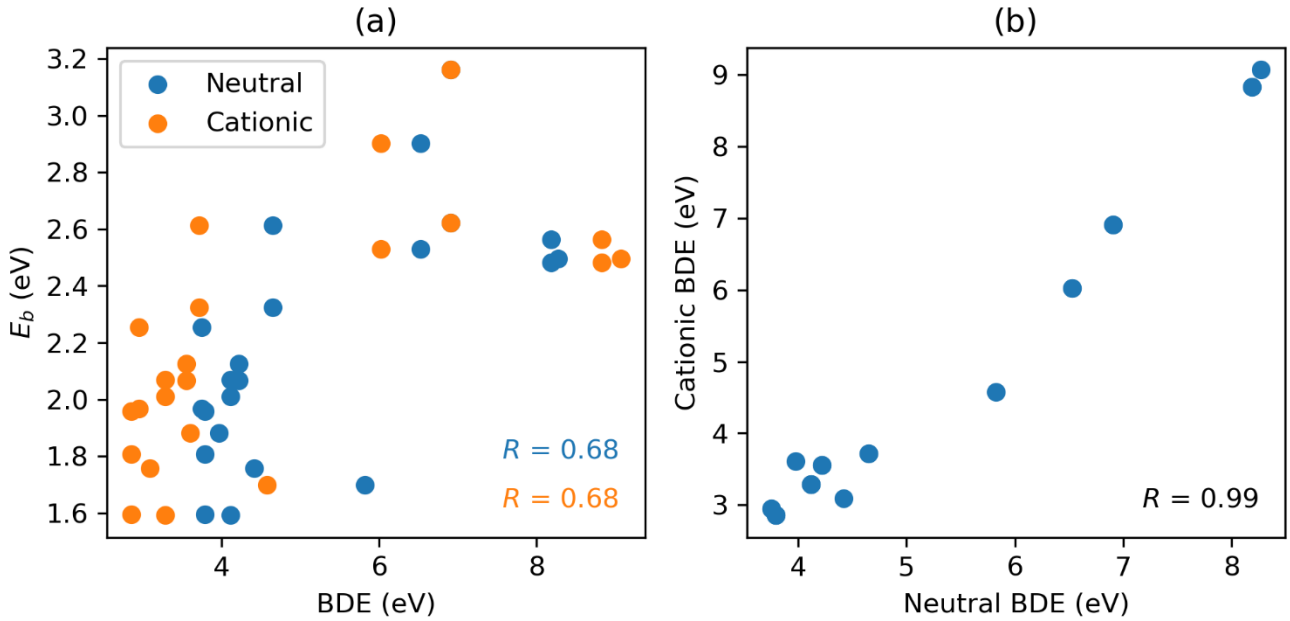

Figure S8. (a) Correlation of experimental bond dissociation energies (BDEs) for neutral diatomic molecules (blue) and diatomic cations (orange) with respect to SCAN+*U*-calculated crystal bond dissociation energies (E_b) showing the difference between molecular and crystal bond strengths. *R* is the Pearson correlation coefficient.[7] (b) Experimental BDEs for neutral diatomic molecules strongly correlate with those of diatomic cations. We tabulated BDEs and E_b in features.csv.

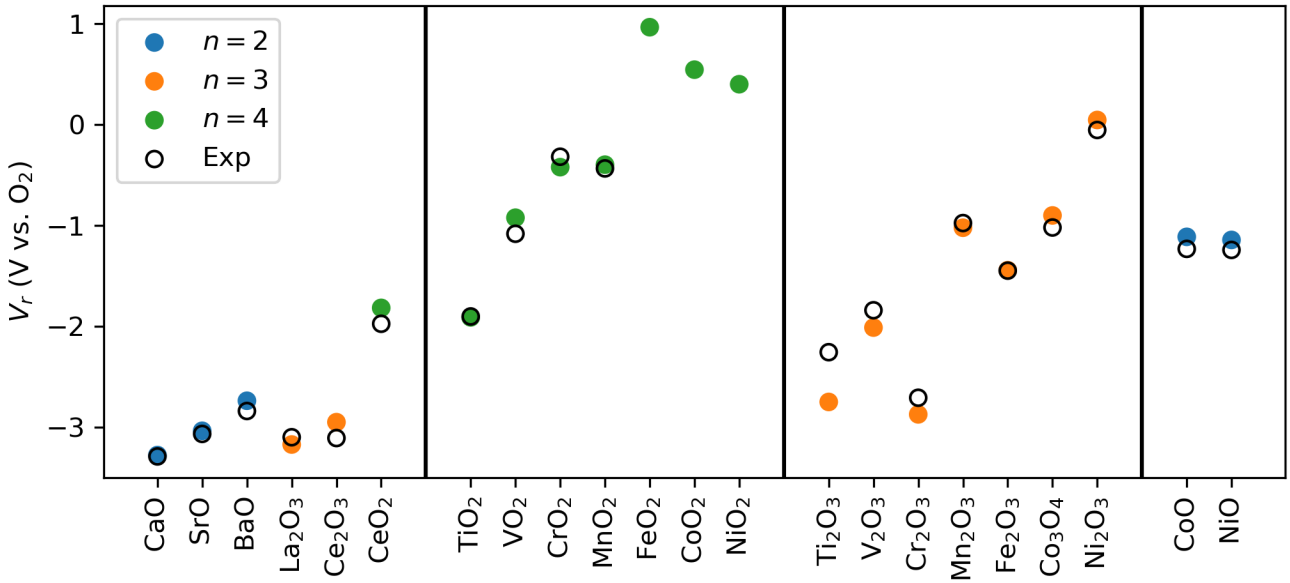

Figure S9. Specific trends in the SCAN+*U*-calculated and experimental V_r vs. (a) A-site atoms (+2/+3/+4), (b) B-site atoms with +4 oxidation state, (c) B with +3, and (d) B with +2. Experimental V_r for FeO_2, CoO_2, and NiO_2 are not available due to the metastability of binary Fe^{4+}, Co^{4+}, and Ni^{4+} oxides. We tabulated V_r in features.csv.

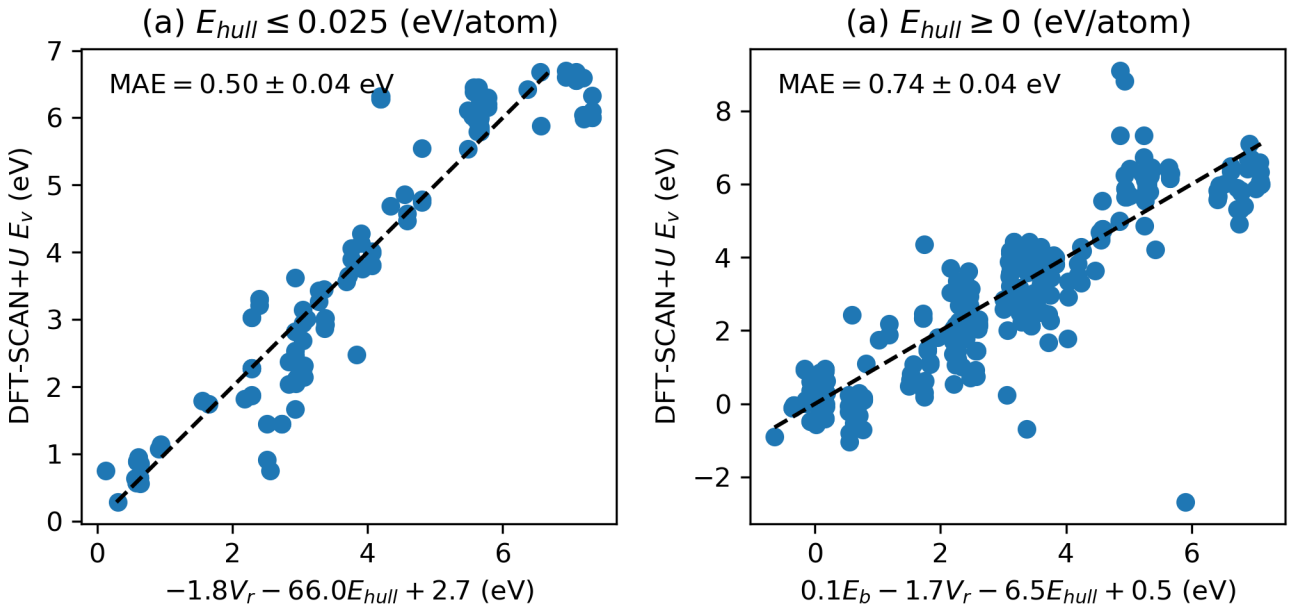

Figure S10. SCAN+*U*-calculated vs. simplified-model-predicted E_v for (a) room-temperature-stable ($E_{hull} \leq 298.15k_B$) and (b) all ABO_3 perovskite structures considered.

References

(1) Wang, L.; Maxisch, T.; Ceder, G. Oxidation Energies of Transition Metal Oxides within the GGA+U Framework. *Phys. Rev. B* **2006**, *73* (19), 195107. https://doi.org/10.1103/PhysRevB.73.195107.

(2) Sai Gautam, G.; Carter, E. A. Evaluating Transition Metal Oxides within DFT-SCAN and SCAN+U Frameworks for Solar Thermochemical Applications. *Phys. Rev. Mater.* **2018**, *2* (9), 095401. https://doi.org/10.1103/PhysRevMaterials.2.095401.

(3) Kittel, C. *Introduction to Solid State Physics*, 8th ed.; McEuen, P., Ed.; Hoboken, NJ: J. Wiley, 2005.

(4) Kubaschewski, O.; Alcock, C. B. *Metallurgical Thermochemistry*, 5th ed.; Raynor, G. V., Ed.; Pergamon Press, 1959; Vol. 12. https://doi.org/10.1063/1.3060816.

(5) Wagman, D. D.; Evans, W. H.; Parker, V. B.; Schumm, R. H.; Halow, I.; Bailey, S. M.; Churney, K. L.; Nuttall, R. L. *Erratum: The NBS Tables of Chemical Thermodynamic Properties. Selected Values for Inorganic and C1 and C2 Organic Substances in SI Units [J. Phys. Chem. Ref. Data 11, Suppl. 2 (1982)]*; Lide, D. R., Ed.; American Chemical Society: Washington, DC, 1989; Vol. 18. https://doi.org/10.1063/1.555845.

(6) Barin, I. *Thermochemical Data of Pure Substances*; Wiley, 1995. https://doi.org/10.1002/9783527619825.

(7) Blyth, S. Karl Pearson and the Correlation Curve. *Int. Stat. Rev. / Rev. Int. Stat.* **1994**, *62* (3), 393. https://doi.org/10.2307/1403769.